GeoHazards

MDPI

*Article*

# Comparative Assessment of Lead Rubber and Friction Pendulum Seismic Isolation Systems Under Varying Seismic Hazard and Site Conditions

**Batuhan Kahvecioğlu [1], Sinan Melih Nigdeli [1], Gebrail Bekdaş [1,*], Sanghun Kim [2] and Zong Woo Geem [3,*]**

[1] Department of Civil Engineering, Istanbul University-Cerrahpasa, Istanbul 34320, Türkiye; batuhan.kahvecioglu@ogr.iuc.edu.tr (B.K.); melihnig@iuc.edu.tr (S.M.N.)
[2] Department of Civil & Environmental Engineering, Temple University, Philadelphia, PA 19122, USA; sanghun.kim@temple.edu
[3] College of IT Convergence, Gachon University, Seongnam 13120, Republic of Korea
* Correspondence: bekdas@iuc.edu.tr (G.B.); geem@gachon.ac.kr (Z.W.G.)

**Abstract**

This study investigates the comparative effectiveness of Lead Rubber Bearing (LRB) and Friction Pendulum System (FPS) isolation units under varying seismic hazard levels and soil classes, within the framework of the Turkish Building Earthquake Code (TBEC 2018). The assessment was conducted in two stages. First, keeping the site class constant, multiple locations characterized by different seismic hazard levels are examined. Second, a fixed geographical location is considered to evaluate the influence of different site classes on isolator response. The performance of the isolation systems is evaluated in terms of displacement demand, base shear ratio, and code-based verification criteria. Additional sensitivity checks were performed using selected limit values to better understand the response trends under changing hazard and soil parameters. The findings highlight how soil amplification effects and seismic intensity levels influence the relative advantages of LRB and FPSs. The results provide practical insight for the selection of seismic isolation systems in hazard-prone regions, contributing to improved performance-based decision-making in earthquake-resistant design. The isolator parameter choices were set based on average catalogue values provided by manufacturers to make this research an example. As a result of the analysis of the isolators' performance, it was concluded that the FPS-type isolator performed better as acceleration values increased.

**Keywords:** seismic isolation; lead rubber bearing; friction pendulum system; TBEC 2018



Academic Editor: Antonio Formisano

Received: 13 May 2026
Revised: 11 June 2026
Accepted: 17 June 2026
Published: 19 June 2026



## 1. Introduction

Throughout the history of civil engineering, one of the greatest threats engineers have faced in structural analysis and applications is the impact of earthquakes. The seismic-resistance concept of designing and constructing buildings has been developed to counter this impact. With advances in technology, applications have emerged to minimize the impact of earthquakes. One of the most effective methods used to reduce the impact of earthquakes on a structure is the seismic isolation system. Seismic isolation systems are used to isolate the structure from its base, which makes the entire structure earthquake-resistant and reduces the risk of damage by extending the structure's natural period [1]. Some of the seismic isolators used in base isolation are the lead core elastomer type and the curved-surface friction-type isolator. The efficiency levels of these two different types

of isolators vary depending on the seismic activity of the region where they are installed. Consequently, isolator selection based on the specific project is a critical consideration. When making this selection, the region must be thoroughly understood, and the suitability of the isolators must be verified against relevant regulations. The aim of this study is to facilitate the selection of appropriate isolators in future projects by analyzing the design checks and results. In this context, the study first keeps the soil class constant and performs analyses using acceleration values obtained from various regions of Türkiye. Then, a specific location in Türkiye is selected, and the behavior of the isolators is examined using accelerations corresponding to the different soil classes defined in TBEC 2018, Section 16.4 [2]. When evaluating the performance of isolators, the following checks defined in TBEC 2018 will be applied: re-centering check, base shear force transferred to the foundation check, deformation checks, and vertical stability checks. In this study, some limit values will be used, such as lower and upper limit values and the base shear force ratio limit. The scope of this study is entirely analytical and models the behavior of these isolators under various design conditions using a specially developed calculation tool derived from the procedures detailed in Chapter 14 of TBEC 2018. To ensure robust conclusions, this study transcends traditional two-point comparisons by employing comprehensive linear regression analysis across the entire parametric database, quantifying system sensitivity through continuous performance slopes. Initial results indicate the existence of critical seismic thresholds at which one type of isolator becomes clearly more advantageous than another, providing a significant perspective for the design selection decision-making process. These analytical findings offer engineers a fundamental, code-compliant guide for selecting the most appropriate type of seismic isolator.

Wu P. and Ou J. [3] demonstrated that existing isolators are insufficient for earthquakes with extremely low occurrence rates due to their deformation limitations and proposed several isolator designs to address this issue. For reinforced concrete structures, Özer E. et al. [4] examined LRB and FPS-type isolators, finding that FPS isolators are more effective at higher displacements while LRB systems exhibit greater sensitivity to torsional effects. Similarly, Hasan Q. F. and Al-Mamany D. A. [5] compared lead core rubber isolators with friction pendulum systems, arguing that the latter deliver superior overall performance. In contrast, Nuraini S. et al. [6] concluded that both isolation types can be used interchangeably without significant performance disparities. This was further supported by Son J. et al. [7] through field tests, which revealed no substantial differences between the two systems regarding equivalent damping ratios. Expanding on these comparative investigations, Vibhute A. et al. [8] provided a comprehensive performance assessment of FPS and LRB isolated frames under mainshock and aftershock sequences, highlighting the critical influence of friction parameters and seismic demand characteristics on the re-centering capability of these systems, which reinforces the necessity of the parametric approach adopted here.

The operational parameters and specific structural applications of these systems have also been widely investigated. Alasaf E. and Öztürk H. [9] evaluated lead core rubber isolators to determine how variations in the characteristic strength ratio and isolation period affect behavior across different soil classes. Zulfakar M. and Karakaş A. İ. [10] compared devices with varying numbers of friction surfaces and reported that three-surface pendulum isolators offer greater design advantages. In terms of building typology, Öztürk M. [11] emphasized that friction-type pendulum systems represent a critical seismic solution under TBEC 2018 guidelines, particularly for high-risk structures such as hospitals. This alignment with critical infrastructure is consistent with the findings of Vilca-Cordova F. et al. [12] for a hospital building in Peru; their upper and lower limit analyses showed that

LRB systems performed better regarding floor accelerations in lower limit states, whereas friction pendulum systems excelled in upper limit analyses.

Furthermore, structural geometry and environmental soil conditions play a decisive role in isolation efficiency. Mohan A. et al. [13] found that the integration of seismic isolation successfully reduces inter-story drift as the number of stories increases. Rajab M. H. et al. [14] examined these systems under 72 distinct structural conditions, noting that friction pendulum isolators effectively minimize story drift, while LRB systems remain highly effective at high frequencies. Under varying seismic demands, Vibhute A. S. et al. [15] evaluated both isolation types under near-fault and far-fault ground motions, observing nearly identical performances. For irregular buildings, dynamic time-domain analyses by Rajput G. and Mishra V. [16] highlighted key period and stiffness advantages, while Shiravand M. R. and Ketabdari H. [17] determined that deploying friction pendulums on exterior columns and LRBs on interior columns optimally minimizes base shear and drift. Additionally, Poornima B. S. and Babu J. B. S. [18] demonstrated the general benefits of isolation in high-seismic zones on medium soil, noting the technical edge of friction systems, while Anand G. et al. [19] identified the lower part of the bridge pier as the most efficient location for bridge isolators. Finally, regarding broader geotechnical risks, a series of comprehensive fragility and nonlinear time-history analyses by Shen Y. et al. [20–22] underscored that the structures cross-cutting or embedded within liquefiable soil deposits face significantly higher seismic damage risks than those in homogeneous non-liquefiable boundaries, highlighting the critical importance of intensity measure selection in capturing continuous maximum acceleration responses.

While numerous comparative studies evaluate the seismic performance of LRB and FPS systems, they often rely on idealized isolator properties or localized, single-site seismic scenarios that fail to capture broader regional variations. This study addresses this scientific gap through a comprehensive macro-level parametric assessment tailored specifically to the structural design framework of the TBEC 2018 guidelines. The primary novelty of this work lies in two distinct aspects: first, rather than using theoretical or arbitrary isolator parameters, the mechanical parameters of both LRB and FPS isolators are derived directly from the statistical averages of contemporary commercial manufacturing catalogues, ensuring a highly realistic representation of practical engineering applications. Second, instead of relying on isolated data point comparisons, this study introduces a comprehensive sensitivity analysis. By systematically evaluating isolator performance across 17 distinct regions that comprehensively represent the seismicity of Türkiye, spanning a wide acceleration spectrum from 0.2 to 1.1, mathematical sensitivity models were established that define the performance of each system as a continuous function of seismic demand. By reporting specific performance slopes and coefficients of determination ($R^2$), this work transitions from qualitative observation to quantitative predictive modeling. Furthermore, by incorporating the complete spectrum of local soil classes for a region, this manuscript provides new, systemic insights into how soil-amplified ground motion demands dictate the definitive operational thresholds and efficiency boundaries of each isolator type. Consequently, this work establishes a rigorous benchmark for selecting optimal isolation systems under diverse regional seismic conditions and complex geotechnical conditions.

Beyond the immediate structural and geotechnical safety domains, the implementation of advanced seismic isolation systems directly aligns with global sustainability paradigms, specifically the United Nations Sustainable Development Goals (UN SDGs). By mitigating post-earthquake structural damage, minimizing debris generation, and preventing the catastrophic loss of material resources, both LRB and FPS technologies contribute directly to SDG 9 (Industry, Innovation, and Infrastructure) and SDG 11 (Sustainable Cities and Communities). Ensuring the continuous functionality of critical infrastructure—such as

hospitals and transit networks—without requiring extensive post-disaster reconstruction fundamentally enhances urban resilience, establishing a clear link between precise technical performance and long-term socio-economic sustainability. Consequently, this study evaluates the structural efficiency of these systems not merely as isolated mechanical mechanisms, but as critical components of resilient urban ecosystems.

## 2. Materials and Methods

Within the scope of this study, the structural characteristics serving as the basis for the analysis were determined to represent an average residential building. The building features a reinforced concrete frame system. The building is designed with a beam–slab floor system for the isolator level and the floors above it, while the level below the isolators is designed with a reinforced concrete foundation. The building consists of 1 isolation floor, 1 basement, a ground floor, and 5 standard floors. The reason for limiting the number of floors to these levels is to prevent excessive tensile forces; in higher-rise and more slender structures, significantly higher tensile forces may occur due to the overturning effect, which negatively impacts the performance of the isolators. A sample plan and cross-sectional view of the structure, which contain a total of 25 isolators, are shown in Figures 1 and 2.

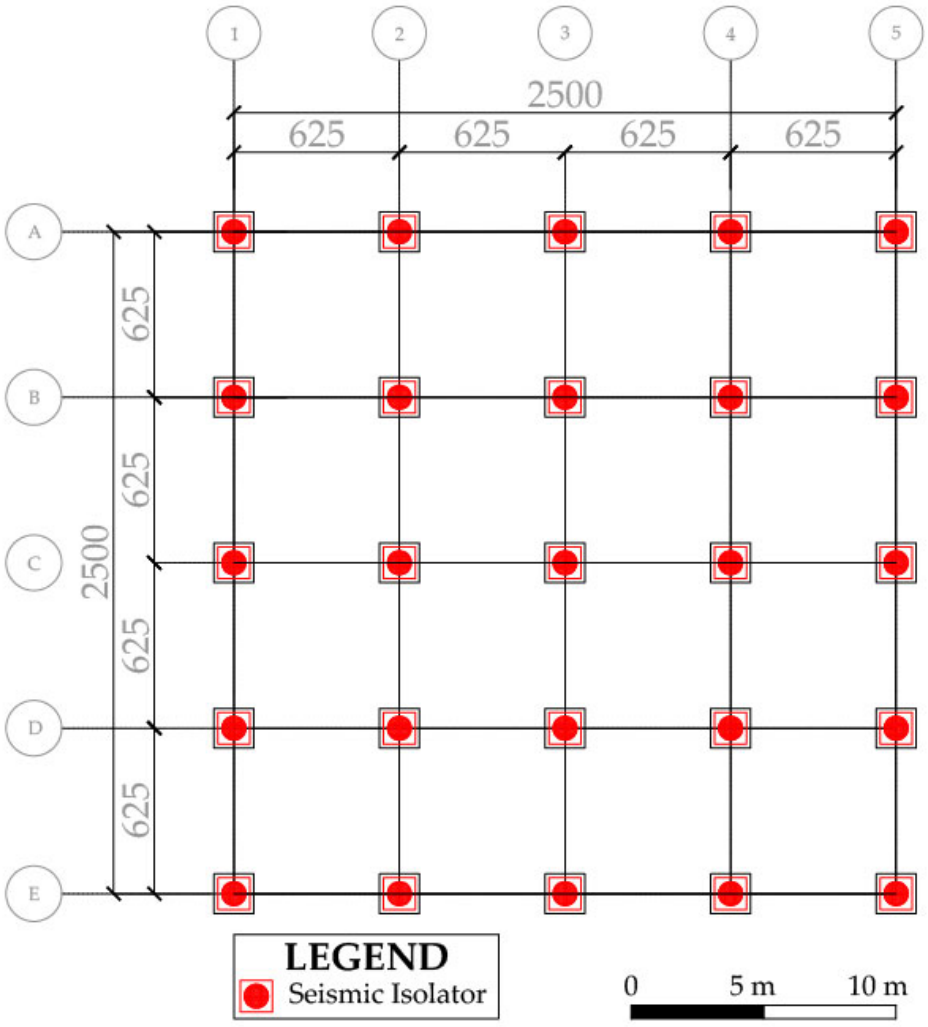


**Figure 1.** Sample floor plan (unit: cm).

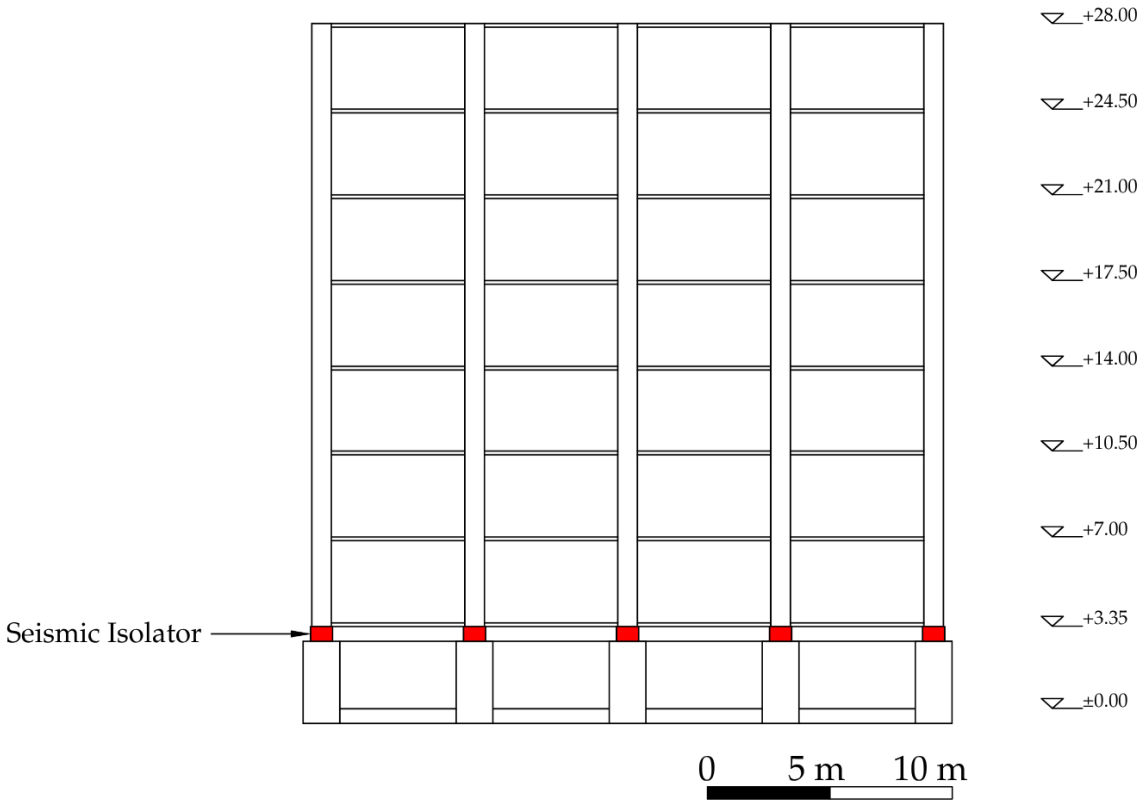


**Figure 2.** Sample cross-section drawing (unit: m).

In this context, taking the structural characteristics under consideration, the axial load values acting on the isolators are, in order: an average of 3000 kN for the 'G + 0.3Q' combination, a maximum of 9000 kN for the '1.4G + 1.6Q' combination ($P_{K1}$), and finally a maximum of 12000 kN for the '1.2G + Q + E' combination ($P_{K2}$). The upper and lower limit values to be used in isolator design checks were selected based on American Society of Civil Engineers guidelines (ASCE 7-22) [23] and are shown in Table 1. The values in Table 1 are the coefficients for isolator parameters such as friction coefficient, post-yield stiffness and characteristic force. Due to aging, dusty conditions, moisture, and other factors, deviations from the original production values may be observed in these parameters with time. For this reason, designs include checks using the lower limit, nominal, and upper limit coefficients for the unlubricated Polytetrafluoroethylene (PTFE) and LRB isolators.

**Table 1.** Upper and lower limit values for isolators.

| Variable | Unlubricated PTFE | Lead Rubber Bearing (LRB) | |
|---|---|---|---|
| | $\mu$ | $K_2$ | $Q_d$ |
| Upper Bound | 1.6 | 1.3 | 1.5 |
| Lower Bound | 0.8 | 0.8 | 0.8 |

In determining the parameters of the friction pendulum-type and lead core rubber-type isolators to be used in this study, data provided by several manufacturers of isolators worldwide were referenced [24–36]. Based on these data, the selected average isolator parameters for the friction pendulum-type and lead core rubber-type isolators are presented in Tables 2 and 3, respectively. These parameters were determined by taking the average of the values listed in the producer catalogs under review and comparing them with parameters that are more commonly used and practical in the industry, thereby establishing

a realistic, market-standard baseline for stock commercial products rather than site-specific custom optimizations. The study highlights that while custom optimization is the industry standard for final project delivery, our framework serves as a critical pre-project engineering screening tool. By benchmarking standard catalog averages, we define the 'base-case' feasibility limits of seismic isolation technology. As a result of the friction pendulum-type investigations, the friction coefficient was selected as 0.045, calculated as the average of the reasonable production and application values of 0.03 and 0.06; similarly, the radius of curvature was selected as 6000 mm. As a result of the lead core rubber-type investigations, the isolator diameter was selected as 900 mm. The reason for this is that the diameter ranges found in the investigations were between 300 mm and 1500 mm on average. After the isolator diameter was specified, the average of the catalog values for a 900 mm diameter from reference producer catalogs was evaluated, resulting in the selection of the following values: 150 mm for the lead core diameter, 0.55 MPa for the shear modulus of rubber, 168 mm for the total rubber thickness, and finally, 7 mm for the single rubber thickness.

**Table 2.** Average parameters of friction-type pendulum isolators.

| Description | Symbol | Unit | Value |
|---|---|---|---|
| Effective Friction Coefficient | $\mu_e$ | - | 0.045 |
| Effective Radius of Curvature of the Sliding Surfaces of the Isolation Unit | $R_C$ | mm | 6000 |

**Table 3.** Average parameters of lead core rubber-type isolators.

| Description | Symbol | Unit | Value |
|---|---|---|---|
| Diameter of the Elastomer Layer Adhered to the Steel Plate | B | mm | 900 |
| Lead Core Diameter | $B_L$ | mm | 150 |
| Shear Modulus of Rubber | $G_V$ | MPa | 0.55 |
| Total Rubber Thickness | $T_r$ | mm | 168 |
| Single Rubber Thickness | t | mm | 7 |

The $S_{M1}$ value (spectral acceleration coefficient [dimensionless] for a 1.0 s period), which is a key parameter in isolator calculations—particularly in displacement checks—was selected from 17 different regions of Türkiye, with an aim of achieving as balanced a distribution as possible within the range of approximately 0.2 to 1.1. The reason for selecting acceleration values within this range is that they are the most commonly observed in Türkiye. Additionally, these values were initially selected under the assumption that the soil class is ZC. The spectra were obtained using the Türkiye Earthquake Hazard Map prepared by the Disaster and Emergency Management Presidency (AFAD) (2018) [37]. The acceleration values were obtained by inputting the latitude and longitude values listed in Table 4 into the map. The selected locations and acceleration values are presented in Table 4.

In addition to these acceleration coefficients, for which the soil class 'ZC' was selected, spectrum values were obtained for different soil classes in the No. 8 region, where both types of isolators performed successfully based on their average parameters. These soil classes are, in order: ZA, ZB, ZC, ZD, and ZE; the resulting acceleration coefficients are presented in Table 5 below. According to TBEC 2018, soil classes are determined based on the average shear velocity of the soil over a 30 m depth starting from below the foundation. Soil classes are named ZA for velocities above 1500 m/s, ZB for velocities between 760 and 1500 m/s, ZC for velocities between 360 and 760 m/s, ZD for velocities between 180 and 360 m/s, and finally ZE for velocities below 180 m/s.

**Table 4.** Selected locations and acceleration values.

| No | Latitude | Longitude | $S_{M1}$ |
|---|---|---|---|
| 1 | 39.175240 | 34.153949 | 0.199 |
| 2 | 37.531771 | 40.887669 | 0.250 |
| 3 | 37.724183 | 40.417025 | 0.285 |
| 4 | 41.046968 | 40.900989 | 0.354 |
| 5 | 37.064856 | 37.378016 | 0.393 |
| 6 | 39.843628 | 30.676337 | 0.453 |
| 7 | 36.519589 | 30.528115 | 0.507 |
| 8 | 37.790413 | 38.286012 | 0.535 |
| 9 | 37.078532 | 27.253575 | 0.609 |
| 10 | 40.182983 | 29.066912 | 0.645 |
| 11 | 39.502359 | 26.979706 | 0.714 |
| 12 | 36.620000 | 29.127351 | 0.747 |
| 13 | 38.194724 | 26.838992 | 0.789 |
| 14 | 37.487591 | 37.293856 | 0.839 |
| 15 | 40.957318 | 28.832127 | 0.909 |
| 16 | 36.489740 | 36.304002 | 0.942 |
| 17 | 40.772718 | 30.393581 | 1.093 |

**Table 5.** Acceleration values for different soil classes.

| | ZA | ZB | ZC | ZD | ZE |
|---|---|---|---|---|---|
| $S_{M1}$ | 0.286 | 0.286 | 0.535 | 0.694 | 0.918 |

Although short-period spectral acceleration coefficients ($S_{DS}$) were also evaluated for all cases, they are omitted from the main tables since the prolonged isolation periods shift the structural demand entirely into the $S_{M1}$-governed region, leaving $S_{DS}$ with no direct numerical impact on the isolator-level limit states.

### *2.1. Design Formulations for Isolators*

This section contains the formulations and explanations from TBEC 2018 that will be used in the scope of the work for FPS and LRB.

#### 2.1.1. Formulations for Friction Pendulum Isolator (FPS)

- Maximum $v/w$ ratio for the substructure

$$V = (S_{ae} * W * \eta)/R, \quad (1)$$

In Equation (1), V represents the force acting on the substructure, $S_{ae}$ represents the spectral acceleration value at the $T_M$ period for the maximum seismic ground motion level, W represents the weight of the building, η represents the damping scaling factor for the maximum ground motion level, and finally, R represents the seismic load reduction factor.

- Re-centering

$$(\mu_e + D_M/R_C) - (\mu_e + (0.5 * D_M/R_C)) > 0.025, \quad (2)$$

In Equation (2), $\mu_e$ represents the effective friction coefficient for the lower-bound value, $D_M$ represents the displacement value that will occur at the effective stiffness center

of the isolation system in the considered direction under the maximum seismic ground motion level, and finally, $R_C$ represents the radius of curvature of the isolation unit's sliding surface.

2.1.2. Formulations for Lead-Rubber-Core Isolator (LRB)

- Maximum $v/w$ ratio for the sub-structure

  The formula in Equation (1) is used for this calculation.

- Re-centering

$$v/w \text{ (for maximum } D_M) - v/w \text{ (for half of the maximum } D_M) > 0.025, \quad (3)$$

- Deformations for $P_{K1}$ combination

$$\gamma_{c,\,st} \leq 3.5, \quad (4)$$

The term $\gamma_{c,\,st}$ in Equation (4) represents the angular deformation caused by pressure.

$$\gamma_{c,\,st} + \gamma_{s,\,st} + \gamma_{r,\,st} \leq 5, \quad (5)$$

In Equation (5), $\gamma_{s,\,st}$ represents the angular displacement caused by horizontal displacement resulting from factors other than earthquakes (expansion, wind, etc.), while $\gamma_{r,\,st}$ represents the unit displacement caused by the relative rotation between the upper and lower plates of the isolation unit.

- Deformations for $P_{K2}$ combination

$$\gamma_{s,\,E} \leq 2, \quad (6)$$

In Equation (6), $\gamma_{s,\,E}$ represents the unit strain value resulting from the horizontal displacement caused by the DD-1 and DD-2 earthquake ground motion effects.

$$\gamma_{c,\,E} + \gamma_{s,\,E} + 0.5\gamma_{r,\,st} \leq 6, \quad (7)$$

In Equation (7), $\gamma_{c,\,E}$ represents the unit strain value resulting from the pressure generated under the influence of the DD-1 and DD-2 ground motion effects.

- Vertical stability

$$\min (P'_{cr}, P_{str})/P_{K2} \geq 1.1, \quad (8)$$

In Equation (8), $P'_{cr}$ represents the buckling load value of the elastomeric isolation units under horizontal displacement, while $P_{str}$ represents the axial load capacity of the elastomeric isolation units associated with unit deformation.

$$\min (P_{cr}, P_{str})/P_{K1} \geq 2, \quad (9)$$

In Equation (9), $P_{cr}$ represents the buckling load value of the elastomeric isolation units in the case where there is no horizontal displacement.

To explicitly define the non-linear lateral behavior and energy dissipation mechanisms of the isolation units investigated in this parametric study, the mathematical models are constructed in accordance with the bilinear hysteretic representation standardized under TBEC 2018 (Section 14A). The cyclic force–displacement (F-D) relationships govern the non-linear structural response under dynamic actions. As a representative benchmark to illustrate these boundary behaviors, the standardized analytical loops for both systems were generated using the actual mechanical outputs under the 0.535 g spectral acceleration ($S_{M1}$) protocol at Location 8 (ZC soil class). The resulting analytical hysteresis loop for the Lead Rubber Bearing (LRB) configuration is depicted in Figure 3.

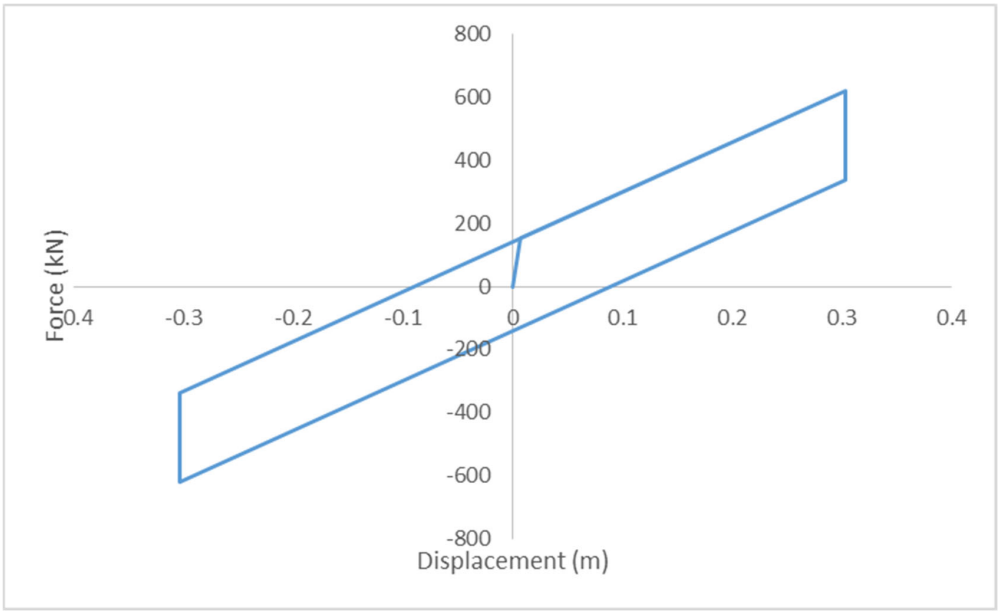


**Figure 3.** Standardized analytical bilinear hysteretic force–displacement loop for the LRB unit under 0.535 g spectral acceleration ($S_{M1}$) for Location 8 (ZC soil class).

As illustrated in Figure 3, the LRB system exhibits a typical bilinear continuum defined in TBEC Section 14A, where the initial elastic stiffness ($k_1$) transitions into a post-yield shear stiffness ($k_2$) once the effective yield displacement ($D_y$) and characteristic strength ($F_Q$) parameters are exceeded, effectively closing the energy dissipation spiral via the continuous lead core yielding.

On the other hand, the Friction Pendulum System (FPS) relies on a rigid-plastic friction threshold combined with a pendulum action climbing a spherical concave surface in accordance with TBEC Section 14B. The secondary stiffness ($k_2$) is directly governed by the ratio of the supported structural weight to the effective curvature radius ($P/R_c$). The corresponding analytical force–displacement response for the FPS configuration under the identical seismic demand (0.535 g, Location 8, ZC) is presented in Figure 4.

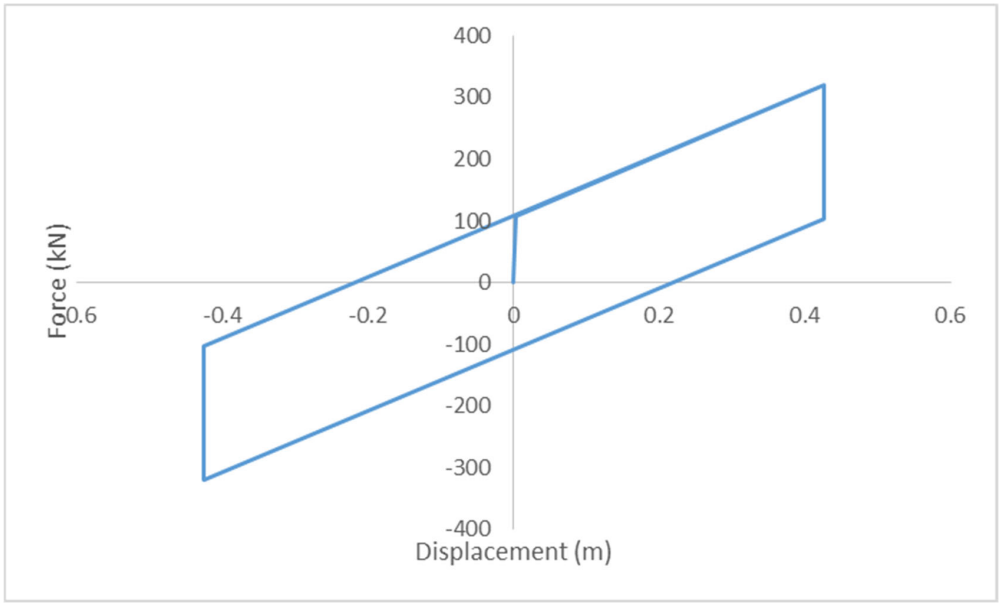


**Figure 4.** Standardized analytical bilinear hysteretic force–displacement loop for the FPS unit under 0.535 g spectral acceleration ($S_{M1}$) for Location 8 (ZC soil class).

## 3. Results

Within the scope of this study, two types of isolators were examined, as shown in Tables 2 and 3. In the initial phase, a study was conducted using the acceleration values listed in Table 4 for these isolators, and the isolators were verified in accordance with TBEC 2018. The checks performed for the friction pendulum-type isolator include the ratio of the base shear force transmitted to the substructure to the structure's weight ($v/w$) and the re-centering check. For the lead-core rubber-type isolators, the checks were, in order: $v/w$, re-centering, deformation checks for the 1.4G + 1.6Q ($P_{K1}$) combination, deformation checks for the 1.2G + Q + E ($P_{K2}$) combination, and vertical stability checks.

Rather than employing iterative commercial finite element software for non-linear time-history simulations, this study utilizes a rigorous analytical framework strictly based on the closed-form engineering formulations mandated by the Turkish Building Earthquake Code (TBEC-2018, Chapter 14). To evaluate and compare the seismic isolation performances, a series of deterministic compliance and stability checks were systematically executed using validated calculation spreadsheets. The reliability of the developed calculation tool was verified by comparing its results with those obtained from the commercial software ETABS v22.6.0 (Computers and Structures, Inc., Walnut Creek, CA, USA) [38]. A benchmark model was established, and the detailed validation process, along with the comparative results for both FPS and LRB systems, is provided in Appendix A.

For both the Lead Rubber Bearing (LRB) and Friction Pendulum System (FPS), the mutual evaluation criteria include the displacement calculations, the base shear force ratio transmitted to the foundation ($v/w$), and the re-centering capability of the isolation system.

Furthermore, system-specific safety checks were performed for the LRB units, explicitly accounting for shear deformation limits under specific vertical load combinations ($P_{K1}$ and $P_{K2}$) and the buckling checks. This analytical methodology represents the benchmark verification practice widely accepted in structural engineering for the preliminary sizing and regulatory compliance evaluation of seismic isolation systems.

Additionally, the effective damping ratios used in the analytical calculations comply with the maximum limits stipulated by the code. In accordance with TBEC-2018, an upper damping constraint of 30% was applied; any effective damping ratio calculated above this threshold was conservatively taken as 30% in subsequent checks.

As a result of the design checks performed across the entire dataset, it was determined that the friction pendulum-type isolator satisfies all relevant code requirements for acceleration values within the range of 6–16 (as listed in Table 4). For the lead core rubber-type isolator, code compliance is achieved within moderate seismic demand levels (e.g., accelerations 7 and 8), a trend that is further quantified and extrapolated through the comprehensive linear regression analysis presented in Section 3.3. To illustrate the underlying performance metrics, the detailed verification checks for both isolator types are presented below, using the 8th acceleration value (0.535 g) as a representative case study. The limit value for the $v/w$ ratio is set at 0.20.

### *3.1. Friction Pendulum-Type Isolator (FPS) Design Checks*

#### 3.1.1. Maximum $v/w$ Ratio Check for the Sub-Structure

Based on Equation (1), $S_{ae}$ is calculated as 0.17 g, W is calculated as 75000 kN, η is calculated as 0.53, and finally, R is taken as 1. Based on the calculations performed, the $v/w$ ratio is calculated as 0.09, which does not exceed the limit value of 0.20, indicating satisfactory performance.

#### 3.1.2. Re-Centering Check

Based on Equation (2), $\mu_e$ is taken as 0.036, $D_M$ is calculated as 0.43 m, and finally, $R_C$ is taken as 6 m. According to the calculations, the re-centering calculation was determined to be 0.04, and this value exceeds the lower limit of 0.025, indicating satisfactory performance.

### *3.2. Lead-Rubber-Core (LRB) Isolator Design Checks*

#### 3.2.1. Maximum $v/w$ Ratio Check for the Sub-Structure

Based on Equation (1), the $v/w$ ratio is calculated as 0.186, which does not exceed the limit value of 0.20.

#### 3.2.2. Re-Centering Check

Based on Equation (3), the re-centering calculation was determined to be 0.034, and this value exceeds the lower limit of 0.025, indicating satisfactory performance.

#### 3.2.3. Deformation Checks for $P_{K1}$ Combination

Based on Equation (4), the result is calculated as 0.85, which gives a positive result as it does not exceed the upper limit of 3.5.

Based on Equation (5), the result is calculated as 2.75, which does not exceed the upper limit of 5 and thus provides a positive result.

#### 3.2.4. Deformation Checks for $P_{K2}$ Combination

Based on Equation (6), the result is calculated as 1.99, which does not exceed the upper limit of 2 and thus provides a positive result.

Based on Equation (7), the result is calculated as 4.94, which gives a positive result as it does not exceed the upper limit of 6.

#### 3.2.5. Vertical Stability Checks

Based on Equation (8), the result is calculated as 1.67, which exceeds the lower limit value of 1.1, indicating satisfactory performance.

Based on Equation (9), the result is calculated as 2.23, which exceeds the lower limit of 2 and provides a positive result.

The design checks shown above refer only to the acceleration value numbered 8, as indicated; however, a study was also conducted for all seismic hazard levels. To represent this study, the general results are presented in Appendix A. In the second phase of the study, the analysis proceeded using the acceleration values for the different soil classes listed in Table 5, and the same steps as in the first phase were followed. As a result of the checks performed, it was determined that, for the friction pendulum-type isolator sample, all relevant checks were made for the acceleration values corresponding to the ZC-D-E soil classes listed in Table 5. It was observed that the lead core rubber-type isolator met the code requirement only for the acceleration value corresponding to the ZC soil class.

To evaluate the mechanical sensitivity of the isolation systems under varying demand levels, a sensitivity analysis was performed by scaling the core axial design loads on the isolators by ±25%. In the first load-scaling scenario, the axial load values from the initial baseline configuration (average 3000 kN for G + 0.3Q, maximum 9000 kN for 1.4G + 1.6Q, and 12,000 kN for 1.2G + Q + E) were increased by 25%, resulting in revised design targets of an average of 3750 kN for G + 0.3Q, a maximum of 11,250 kN for 1.4G + 1.6Q, and 15,000 kN for 1.2G + Q + E. Additionally, to observe the impact of reduced axial load values, another scenario was examined, and a new combination was created. In this second load-scaling scenario, the direct impact of a reduced gravity load demand was examined by decreasing the baseline axial forces by 25%, yielding adjusted load profiles of an average of 2250 kN for G + 0.3Q, a maximum of 6750 kN for 1.4G + 1.6Q, and 9000 kN for 1.2G + Q + E. In summary,

these adjustments provide a controlled ±25% variation in the axial load per isolator to observe the system limits without altering superstructure dynamic variables. As a result of the design checks performed, it was observed that increasing or decreasing the axial load per isolator by 25% had no effect on displacement, the $v/w$ ratio, or re-centering for friction pendulum-type isolators. When the effect of changes in axial load values per isolator on lead core rubber-type isolators was examined, it was observed that this change affected the isolator design checks. A 25% increase in axial loads caused an increase in displacement values, and this increase was 19% on average. The effect of the load increase on the $v/w$ check was positive due to the increase in the weight of the structure, and this positive effect was observed to be an average of 10%. In the re-centering checks, the effect of the load increase on this check was positive, with an average of 3%. For the $P_{K1}$ combination, negative effects of 25% and 8%, respectively, were observed in the deformation checks. For the $P_{K2}$ combination, negative effects of 19% and 43% were observed in the deformation checks, respectively. Finally, the effect of a 25% increase in axial loads on buckling checks was examined, and the effect of the load increase on buckling checks was observed to be negative at a rate of 40%. When a 25% decrease in axial loads was examined, the decrease in loads caused a decrease in displacement values, with this decrease being 19% on average. The effect of the load decrease on the $v/w$ check was negative due to the decrease in the weight of the structure, and this negative effect was observed to be 15% on average. In the re-centering checks, the effect of the load decrease on this check was positive on average by 5%. In the deformation checks for the $P_{K1}$ combination, positive effects of 26% and 8%, respectively, were observed. In the deformation checks for the $P_{K2}$ combination, positive effects of 20% and 31%, respectively, were observed. Finally, the effect of a 25% decrease in axial loads on buckling checks was examined, and the effect of the load decrease on buckling checks was observed to be positive at approximately 106%. When the effects of load changes were examined, it was observed that lead core rubber-type isolators could be affected both positively and negatively by this condition; the results for the structural type shown in Figures 1 and 2, which provided more positive results in Section 4, were analyzed. The average isolator parameters listed in Tables 2 and 3, with accelerations from 17 different locations selected in Türkiye and 5 different soil classes for one location, have been controlled by specific regulations. The selected average isolator parameter values were determined by reviewing the catalogs of a total of 13 different isolator producers. A total of 22 different scenarios for 2 different isolator types were analyzed within the scope of the study, and the details are shared in Section 3.3.

### 3.3. Statistical Sensitivity and Linear Regression Analysis

To investigate the continuous sensitivity of the isolation systems and satisfy rigorous statistical validation, a comprehensive linear regression analysis was executed across the entire parametric database. The precise sensitivity slopes (representing the rate of change per unit acceleration, g) and the corresponding coefficients of determination ($R^2$) are consolidated in Table 6.

**Table 6.** Linear regression parameters (slopes and $R^2$) for isolation systems under regional seismicity (phase 1) and soil conditions (phase 2).

| Phase/Structural Check | FPS Slope | FPS $R^2$ | LRB Slope | LRB $R^2$ |
|---|---|---|---|---|
| Phase 1: Regional Seismicity (17 Sites, ZC) | | | | |
| Max. Displacement ($D_{TM}$) | 158.98 | 0.9825 | 103.47 | 0.9914 |
| Base Shear Ratio ($v/w$) | 0.1512 | 0.9456 | 0.4112 | 0.9821 |
| Re-Centering Check | 0.1203 | 0.9805 | 0.1362 | 0.9896 |

**Table 6.** *Cont.*

| Phase/Structural Check | FPS Slope | FPS $R^2$ | LRB Slope | LRB $R^2$ |
|---|---|---|---|---|
| Deformation-$P_{K1}$ (Check 1) | — | — | 0 | 0 |
| Deformation-$P_{K1}$ (Check 2) | — | — | 0 | — |
| Deformation-$P_{K2}$ (Check 1) | — | — | 6.1579 | 0.9912 |
| Deformation-$P_{K2}$ (Check 2) | — | — | 25.683 | 0.6612 |
| Buckling (Check 1) | — | — | −3.793 | 0.9972 |
| Buckling (Check 2) | — | — | −5.0457 | 0.9974 |
| Phase 2: Soil Classes (Site 8, ZA to ZE) | | | | |
| Max. Displacement ($D_{TM}$) | 152.89 | 0.9882 | 102.72 | 0.9947 |
| Base Shear Ratio ($v/w$) | 0.1407 | 0.9563 | 0.3955 | 0.988 |
| Re-Centering Check | 0.1161 | 0.9874 | 0.1357 | 0.9952 |
| Deformation-$P_{K1}$ (Check 1) | — | — | 0 | — |
| Deformation-$P_{K1}$ (Check 2) | — | — | 0 | — |
| Deformation-$P_{K2}$ (Check 1) | — | — | 6.0645 | 0.9955 |
| Deformation-$P_{K2}$ (Check 2) | — | — | 27.033 | 0.7927 |
| Buckling (Check 1) | — | — | −3.8186 | 0.9996 |
| Buckling (Check 2) | — | — | −5.0914 | 0.9996 |

- Regional Seismicity Trends (Phase 1: 17 Locations, Site Class ZC)

As detailed in Table 6, the structural responses of both systems exhibit an extremely high, deterministic positive correlation ($R^2 \geq 0.94$) with the spectral acceleration demand ($S_{M1}$). The maximum torsional displacement ($D_{TM}$) increases linearly under rising hazards, with the FPS configuration showing a steeper sensitivity slope of 158.98 cm/g ($R^2$ = 0.9825) compared to the LRB configuration's slope of 103.47 cm/g ($R^2$ = 0.9914). This lower displacement sensitivity of the LRB is mechanically governed by its higher baseline lateral stiffness. In terms of force transfer, the base shear ratio ($v/w$) of the LRB is highly sensitive to seismicity increments, progressing at a steep slope of 0.4112/g ($R^2$ = 0.9821) and violating the regulatory upper limit of 0.20 in high-hazard zones. Conversely, the FPS configuration maintains a remarkably stable and shallow transfer slope of 0.1512/g ($R^2$ = 0.9456), ensuring safe code compliance across all 17 locations. Regarding the re-centering criteria, both systems improve systematically with rising hazard intensities, yielding compliance slopes of 0.1203/g ($R^2$ = 0.9805) for FPS and 0.1362/g ($R^2$ = 0.9896) for LRB. Crucially, the regression metrics for the LRB-specific sub-component checks expose distinct behavior state trends. The non-seismic deformation limits under the $P_{K1}$ combination yield a slope of 0, proving to be perfectly insensitive to seismic acceleration increments due to being governed strictly by gravity-induced dead and live load configurations. Conversely, the critical seismic performance metrics under the $P_{K2}$ combination scale aggressively with rising $S_{M1}$ levels, exhibiting a slope of 6.1579/g ($R^2$ = 0.9912) for Check 1 and 25.683/g ($R^2$ = 0.6612) for Check 2. Furthermore, the buckling safety margins diminish linearly with steep negative slopes of −3.793/g and −5.0457/g ($R^2 \geq 0.99$). This quantitative progression highlights that standard stock elastomeric bearings exhibit dangerously narrow operational boundaries under severe regional seismicity.

- Geotechnical Soil Amplification Trends (Phase 2: Site 8, ZA to ZE Classes)

The regression profiles across the soil classes reinforce the vulnerability of mass-produced catalog options under local site amplification. Notably, due to identical local soil amplification factors mandated by TBEC 2018 for high-competence rock strata, the ZA and ZB site classes yield identical $S_{M1}$ hazards, resulting in overlapping data points at the baseline of the regression continuum. As the soil profiles soften progressively toward the ZE stratum, the local site amplification drives a drastic surge in design demands. The FPS configuration reliably utilizes its pendulum flexibility to accommodate these amplified horizontal displacements, maintaining a displacement slope of 152.89 cm/g ($R^2$ = 0.9882) and a remarkably controlled base shear slope of 0.1407/g ($R^2$ = 0.9563). In stark contrast, the LRB configuration's sub-component checks display a severe vulnerability to soil softening. While the $P_{K1}$ checks remain unamplified (slope of 0), the sensitivity slopes for the $P_{K2}$ deformation checks surge to 6.0645/g ($R^2$ = 0.9955) and 27.033/g ($R^2$ = 0.7927), respectively. Coupled with aggressive buckling safety degradation slopes ($-3.8186$/g and $-5.0914$/g, $R^2 \geq 0.99$), these structural trends quantitatively demonstrate that mass-produced LRB catalog options fail to satisfy the paired shear strain and stability limits ($\gamma_{s,E} \leq 2$ and buckling criteria) in geotechnical profiles softer than ZB, making site-specific custom optimization mandatory.

As summarized in Table 7, the operational compliance of both isolators is strictly defined by specific seismic intensity thresholds. For FPS units, the system fails to satisfy re-centering requirements in low-seismicity regions ($S_{M1} \leq 0.393$ g) and encounters base shear limitations at extreme hazards ($S_{M1} \geq 1.093$ g). Conversely, LRB units exhibit a significantly narrower compliance window; the system is governed by re-centering failures in low-seismicity zones and suffers from simultaneous $v/w$ ratio, buckling, and $P_{K2}$-deformation violations at intensities exceeding $S_{M1}$ = 0.609 g. This breakdown illustrates that LRB performance is highly sensitive to the interaction between vertical load combinations and lateral displacement demands.

**Table 7.** Seismic compliance and failure modes per $S_{M1}$ intensity.

| Isolator Type | $S_{M1}$ Range (g) | Compliance Status | Governing Limit State (Fail) |
|---|---|---|---|
| FPS | 0.199–0.393 | FAIL | Re-centering |
| FPS | 0.453–0.942 | PASS | - |
| FPS | 1.093 | FAIL | $v/w$ Ratio |
| LRB | 0.199–0.453 | FAIL | Re-centering |
| LRB | 0.507–0.535 | PASS | - |
| LRB | 0.609–1.093 | FAIL | $v/w$, Deformation, Buckling |

## 4. Discussion

While seismic isolation performance is inherently dependent on the full design spectrum and potential near-fault pulse effects, this framework intentionally utilizes $S_{M1}$ as the governing seismic intensity measure. This choice is strictly aligned with the TBEC 2018 methodology, which dictates $S_{M1}$ as the primary parameter for determining displacement demands and base shear in the long-period range. As this study focuses on a macro-level parametric comparison across multiple regions, $S_{M1}$ provides the most robust and consistent intensity measure for evaluating code-compliant isolator performance.

This section contextualizes the analytical findings of the current study within the framework of the existing literature and outlines strategic directions for future research.

When the deformation results for the LRB isolator were examined in the study and quantified through comprehensive linear regression analysis under seismic increments (as summarized in Table 6), deformations occurred when the acceleration threshold of 0.609 g was exceeded using the standard manufacturer parameters (the displacement value corresponding to this threshold is 41 cm). Physically, this represents a significant increase in the shear deformation demands of elastomeric bearings under combined seismic and maximum axial loads, with regression slopes (e.g., 25.683/g for $P_{K2}$-Check 2) indicating a rapid escalation in deformation metrics that eventually violate the strict limit states of TBEC 2018. A study in the literature has also shown that existing isolators are inadequate for earthquakes with an extremely low occurrence rate due to their deformation limitations [3]. This limitation is explicitly manifested in the analytical findings of the current study, particularly under the exceptional $P_{K2}$-b regional hazard scenario (as depicted in Figure A7), where the deformation demands spike dramatically to approximately five times the acceptable design baseline threshold (reaching a value of nearly 30 against the upper limit of 6). This dramatic surge in deformation demands is primarily driven by the severe increase in the acceleration value of the $P_{K2}$ profile, which generates an overwhelming seismic demand that causes standard stock catalog configurations to become structurally untenable under such extraordinary shaking intensities.

When examining the performance of FPS and LRB isolators based on displacement, it was observed that the LRB isolator struggled to meet the required conditions after a displacement of 41 cm, whereas the FPS isolator continued to perform well up to a displacement of 121 cm. This behavioral trend is reflected in Table 6, where the displacement sensitivity of FPS is characterized by a regression slope of 152.89 cm/g under soil class variations. A similar finding was also observed in a previous study, which noted that FPS isolators are more effective at higher displacements [4].

However, some other studies have indicated that both types of isolators perform similarly [6,7]. This variance in the literature is highly reasonable because isolators can often be adapted through adjustments to their parameters; however, since the current study compares standard product parameters, these discrepancies in comparative observations are predictable. It should also be noted at this stage that while revising isolator parameters may lead to positive results for some checks, such revisions generally have negative effects in terms of product cost and production time. From a scalability and practical implementation perspective, relying on non-standard, customized isolator designs introduces significant challenges, including specialized prototype testing, complex quality control procedures, and extended manufacturing lead times. Furthermore, cost–performance considerations dictate a strict trade-off in practice: while modifying geometry or material characteristics might optimize a specific regulatory limit state, it exponentially drives up the initial structural investment. Utilizing standardized manufacturer catalogs, as investigated across the diverse regional and soil scenarios in this study, provides a highly cost-effective, generalized and scalable engineering path by balancing safety compliance with economic feasibility. Additionally, it must not be forgotten that while one check specified in the regulation may be improved, another may be negatively affected. For example, an adjustment made to increase damping may reduce displacement and resolve deformation issues, but in some cases, this can reduce the ability to re-center. This trade-off is clearly reflected in the quantitative metrics of Table 6: as indicated by the regression slopes in Table 6, an increase in seismic demand drives an unfavorable displacement sensitivity of 103.47 cm/g and a sharp surge in deformation demands (slope of 25.683/g for $P_{K2}$-Check 2). Simultaneously, this sensitivity trend forces a positive increase in the re-centering calculations (slope of 0.1362/g), thereby enabling the systems to satisfy the minimum 0.025 threshold mandated by TBEC 2018 under severe shaking. For this reason, this study proceeded using standard parameters.

When evaluating the base shear force transferred to the structure by FPS and LRB isolators, it was observed that FPS isolators transfer approximately half the base shear force to the structure compared to LRB isolators. This finding supports the notion, presented in another study, that friction pendulum systems provide a critical seismic solution, particularly for high-risk structures such as hospitals [11].

The current study examined the compliance of standard isolator parameters with TBEC 2018; however, the evaluations were confined to isolator-level verifications using analytical formulations based on idealized structural models. To account for torsional effects within this framework, the maximum displacement demands were scaled using the 1.1 amplification factor mandated by TBEC 2018, thereby incorporating regulatory eccentricity considerations. However, full structural torsional coupling and near-fault velocity-pulse impacts—which can physically amplify instantaneous energy demands and displacement responses beyond standard code expectations—were outside the baseline scope of this study. To extend the boundaries of these findings and address these limitations, future research directions will focus on conducting comprehensive macro-level evaluations of the entire isolated superstructure. For this purpose, it is planned to establish fully detailed 3-D macro-models in advanced structural analysis programs to execute comprehensive nonlinear time-history analyses, thereby verifying the superstructure–isolation interface dynamically under near-fault pulse suites and complex multi-directional torsional behavior.

Based on the comprehensive analysis of the 17-site dataset, distinct performance boundaries have been identified for both isolator types. It is observed that the performance of the isolator systems is fundamentally driven by the site-specific spectral acceleration ($S_{M1}$), which inherently incorporates the effects of location and soil classification. In this context, the FPS configuration was found to satisfy all regulatory requirements within a broad $S_{M1}$ range of 0.453 g to 0.942 g. Conversely, the LRB configuration was identified to provide full compliance only within a significantly narrower $S_{M1}$ interval ($0.507\ g \leq S_{M1} \leq 0.535\ g$). These performance envelopes, mapped directly against $S_{M1}$ demand, are synthesized into the decision framework presented in Figure 5. It must be noted, however, that these operational boundaries are derived from specific structural models and isolator parameters utilized in this study. Therefore, the proposed framework should be regarded as a conceptual benchmark, and site-specific non-linear verification—as mandated by TBEC 2018—remains essential for final engineering design.

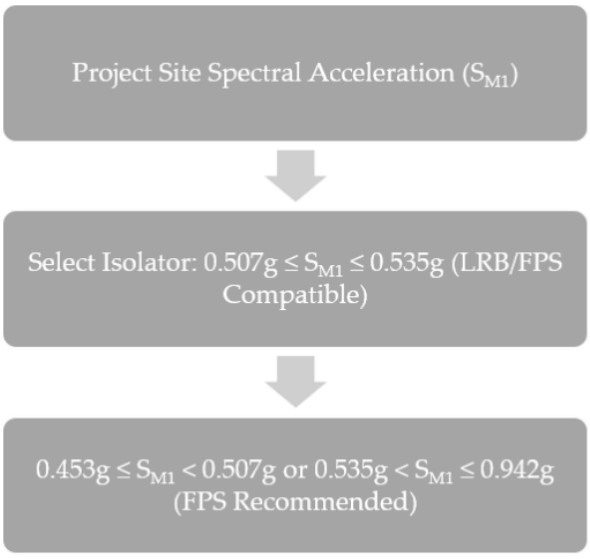


**Figure 5.** Decision framework for seismic isolator selection based on site-specific $S_{M1}$ demand. Note: This framework is constrained by the study parameters. Site-specific verification is mandatory for final design.

Furthermore, this analytical framework is conceptually aligned with physics-informed decision-making models under uncertainty (Sarfarazi S. et al. [39]). While the study relies on standard manufacturer-catalog parameters for scalable preliminary design, it is recognized that the actual seismic performance of isolators is subject to environmental and material uncertainties. To address these, our framework acknowledges the significance of property modification factors to account for friction variability [40], as well as the long-term durability assessments observed in field studies [41]. These considerations, combined with established mechanical principles [42], serve to bridge the gap between catalog-based data and robust, code-based engineering practice. By integrating this systematic screening, we provide an auditable and transparent procedure that manages inherent uncertainties, while emphasizing that site-specific non-linear verification remains mandatory for final engineering design.

The selection framework is summarized in Figure 5, where the performance boundaries are delineated based on the $S_{M1}$ demand. In this schema, the compatibility intervals for FPS and LRB configurations are classified, and the necessity for site-specific verification is underscored for values outside these calibrated ranges.

It must be strictly emphasized that the comparative performance trends presented in this study, specifically the operational compliance boundaries defined for LRB and FPS units (Figure 5), are contingent upon the assumed structural mass, axial load profiles, and average manufacturer-catalog parameters. These findings do not suggest an intrinsic technological superiority of one system over the other. Rather, they serve as a 'performance sensitivity landscape'—a diagnostic tool for preliminary screening. Variations in design parameters, such as lead core dimensions or friction surface geometry, may significantly shift these operational envelopes; thus, final engineering decisions must rely on project-specific non-linear verification.

## 5. Conclusions

The findings of this study, systematically validated through linear regression analysis (Table 6), demonstrate that the compliance of isolation systems is inherently linked to site-specific seismic demand. As seen in the results obtained in this study, some results that do not comply with the regulations were encountered in isolator calculations due to changes in acceleration caused by variations in location and soil class. When compared to previous studies, this research found similar results; for example, as seismicity increases, the friction pendulum-type isolator becomes more effective in this study as well. However, the lead-core rubber isolator can also provide effective performance up to a reasonable displacement threshold through modifications of the parameters. As previously noted, the study proceeded using average isolator parameters; therefore, the negative results observed in the current situation apply to isolators designed using these parameters. It is often possible to obtain results compliant with regulations by modifying various parameters for both FPS and LRB isolators. However, while these modifications often help ensure one type of check, they can negatively affect other checks. For example, while increasing damping to reduce displacement may make the deformation check easier in some cases, it can negatively affect the re-centering check and the $v/w$ ratio. This behavioral trade-off is not incidental but follows the deterministic sensitivity trends established in our regression analysis (Table 6), confirming that optimizing one parameter often entails measurable costs in other regulatory limits. Therefore, it is more appropriate to carefully determine the optimal values for isolator parameters and complete the design accordingly.

The main conclusion of this study is that standard isolator parameters may struggle to satisfy code requirements beyond certain acceleration levels; therefore, isolator manufacturers must base their standards and isolator mold designs on the seismic hazard levels and

soil class of the project's location. Additionally, the engineer responsible for isolator design must continue their work in accordance with the specific location and soil class. While this study establishes a baseline through isolator-level analytical evaluations, full structural torsional coupling and near-fault pulse dynamics remain outside its scope. Future investigations will therefore focus on advanced 3-D nonlinear dynamic simulations of the entire superstructure to comprehensively verify these isolation systems under multi-directional and pulse-type seismic actions.

**Author Contributions:** Conceptualization, S.M.N. and B.K.; methodology, B.K. and G.B.; software, B.K.; validation, S.M.N.; formal analysis, B.K.; investigation, B.K.; writing—original draft preparation, B.K.; writing—review and editing, S.M.N., S.K., Z.W.G. and G.B.; visualization, B.K.; supervision, G.B. and Z.W.G. All authors have read and agreed to the published version of the manuscript.

**Funding:** This research received no external funding.

**Data Availability Statement:** The original contributions presented in this study are included in the article. Further inquiries can be directed to the corresponding authors.

**Acknowledgments:** During the preparation of this manuscript, the authors used GenAI for language refinement. The authors have reviewed and edited the output and take full responsibility for the content of this publication.

**Conflicts of Interest:** The authors declare no conflicts of interest.

## Abbreviations

The following abbreviations are used in this manuscript:

| | |
|---|---|
| LRB | Lead Rubber Bearing |
| FPS | Friction Pendulum System |
| TBEC | Turkish Building Earthquake Code |
| ASCE | American Society of Civil Engineers |
| PTFE | Polytetrafluoroethylene |
| AFAD | Afet ve Acil Durum |

## Appendix A

As illustrated in Figure A1, an increase in acceleration leads to a proportional increase in displacements. However, the systems diverge significantly as the seismicity increases. Under the maximum acceleration of 1.093 g, the FPS exhibits a displacement of 152 cm, compared to 98 cm for the LRB. This trend highlights a critical design trade-off: while the lower horizontal stiffness of the FPS (14.451 N/mm) effectively elongates the fundamental period to reduce base shear, it necessitates a larger seismic isolation gap (clearance) at the foundation level. In contrast, the higher horizontal stiffness of the LRB (44.123 N/mm) serves as a displacement-control mechanism, restricting horizontal movement at the cost of higher acceleration transmission to the superstructure.

As illustrated in Figure A2, the FPS configuration maintains compliance with the TBEC 2018 limit ($v/w \leq 0.20$) for the vast majority of the analyzed seismic spectrum. It is noted that at the extreme seismic demand of 1.093 g, the FPS ratio slightly exceeds the limit, reaching 0.205. While this marginal exceedance suggests that both systems eventually encounter capacity limitations under very high seismic intensities, the FPS exhibits significantly higher stability in base shear ratio compared to the LRB. The LRB system exhibits a performance transition at a seismic intensity of approximately 0.609 g, beyond which it exceeds the allowable $v/w$ ratio more rapidly. This divergence serves as a definitive design boundary: for regions characterized by high seismic hazard ($S_{M1} > 0.60$ g), the FPS system inherently provides a more robust mechanism for base shear ratio, whereas

the application of either system under very high demands necessitates specialized design modifications to ensure full regulatory compliance.

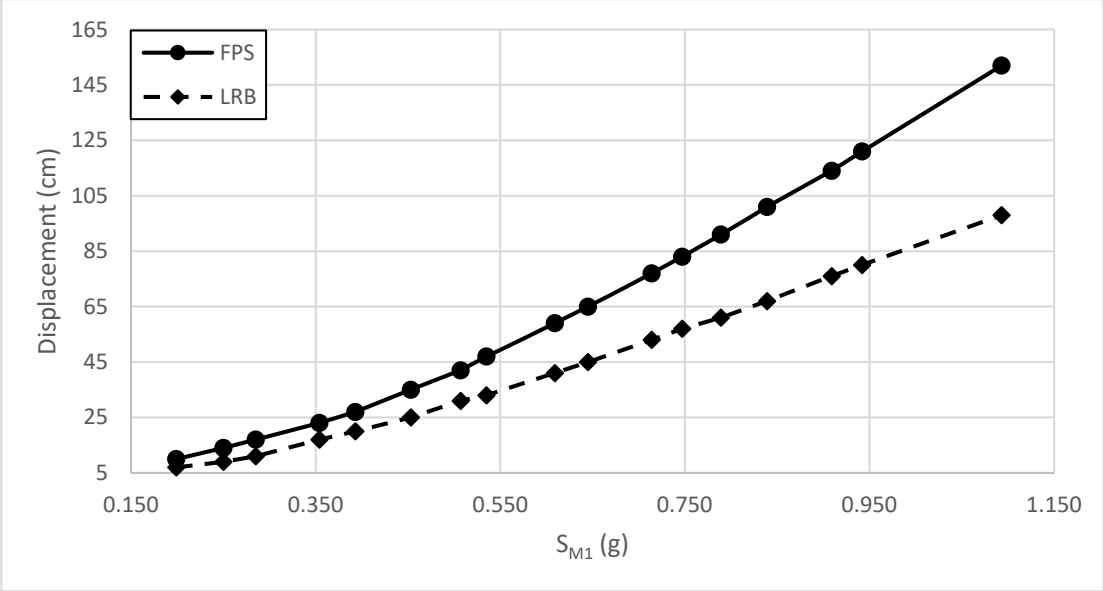


**Figure A1.** $S_{M1}$—Displacement graph.

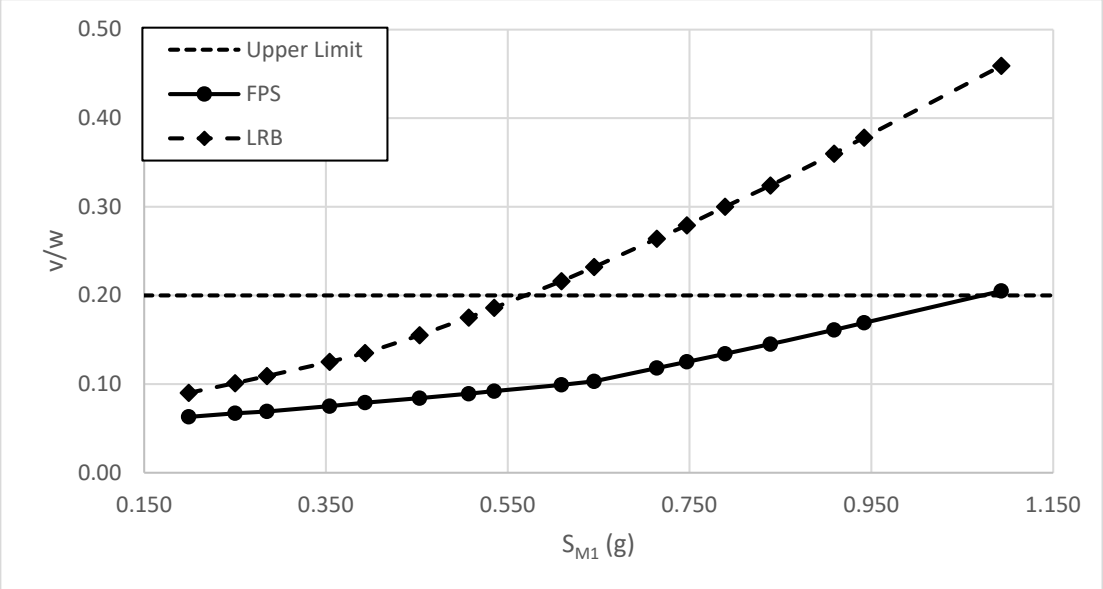


**Figure A2.** $S_{M1}$—$v/w$ Graph (Note: The major horizontal gridline corresponding to the value of 0.20 represents the regulatory upper limit for the $v/w$ ratio as mandated by TBEC 2018).

As illustrated in Figure A3, both systems exhibit a clear dependence on seismic intensity for effective re-centering. Specifically, the FPS configuration achieves compliance with the TBEC 2018 lower limit (0.025) starting from a seismic intensity of 0.453 g, whereas the LRB configuration reaches this threshold at 0.507 g. This behavior is inherently linked to the unique restoration mechanism of each system: while the FPS relies on its concave surface geometry to provide re-centering, the LRB's performance is governed by the lateral shear stiffness of the rubber layers. Below these respective acceleration thresholds, the internal frictional forces and hysteretic damping dominate the restoring force, which explains why the re-centering requirement is not satisfied in low-seismicity regions.

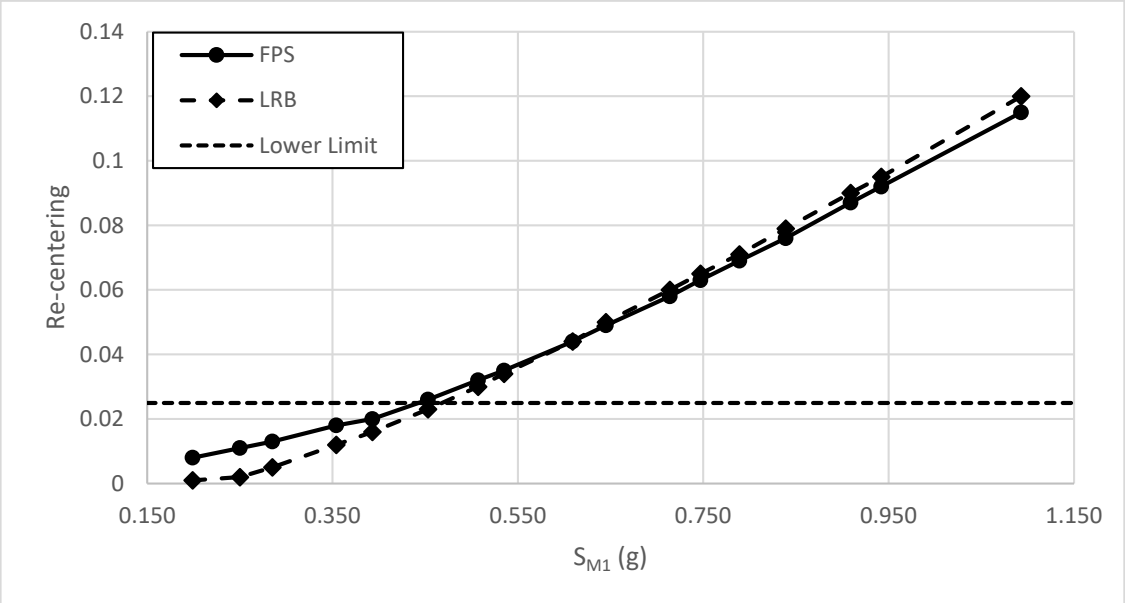


**Figure A3.** $S_{M1}$—Re-centering Graph (Note: The major horizontal gridline corresponding to the value of 0.025 represents the strict regulatory lower limit for the re-centering as mandated by TBEC 2018).

The graphs shown in Figures A4–A9 present the TBEC 2018 checks for each acceleration value listed in Table 4. The horizontal lines in the graphs represent the limit values. The calculations performed using acceleration number 17 in Table 4 were not included in the graphs because the results were mathematically undefined. The reason for this is the following equations used in the calculation of the load-bearing surface area ($A_{re}$) in the displacement condition, where a single elastomer layer is bonded to a steel plate for the $\gamma_{c,E}$, $P'_{cr}$, and $P_{str}$ calculations as required by TBEC 2018.

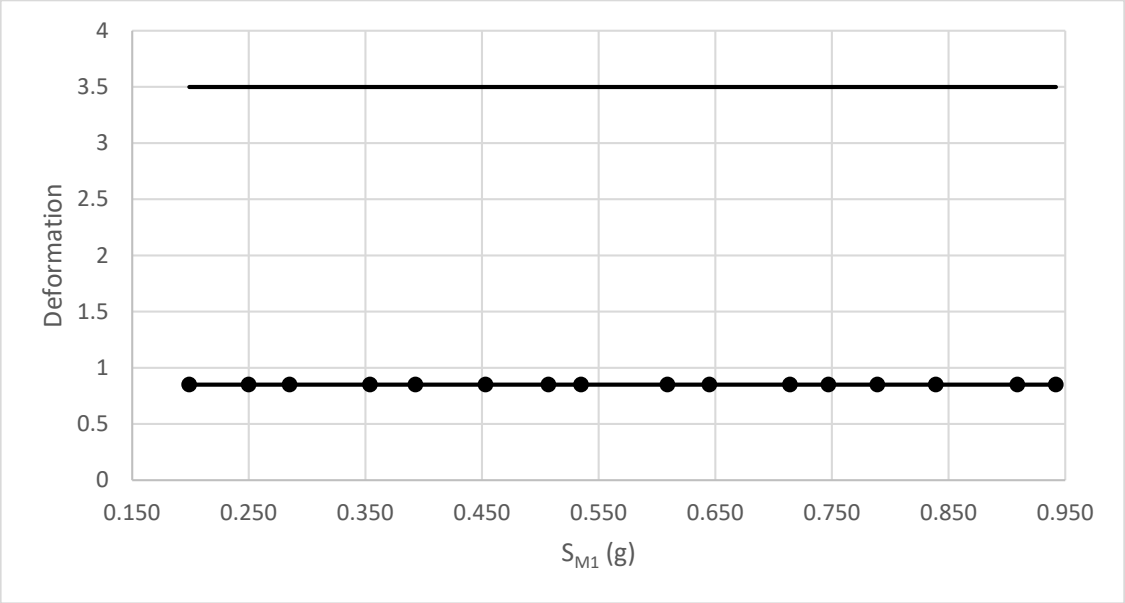


**Figure A4.** $S_{M1}$—Deformation ($P_{K1}$ a) (LRB) (Note: The major horizontal gridline corresponding to the value of 3.5 represents the strict regulatory upper limit for the deformation as mandated by TBEC 2018).

$$A_{re} = A_r * ((\delta - \sin\delta)/\pi)), \quad \text{(A1)}$$

$$\delta = 2\cos^{-1}(D/B), \quad \text{(A2)}$$

As shown in Equations (A1) and (A2), an undefined result is obtained when the ratio of displacement to isolator diameter (D/B) exceeds 1. Since the isolator diameter used in this study is 900 mm, this undefined result occurs as soon as the displacement value exceeds 900 mm. Even if the mentioned undefined condition does not occur and the relevant values can be calculated, the isolators will not perform the relevant checks.

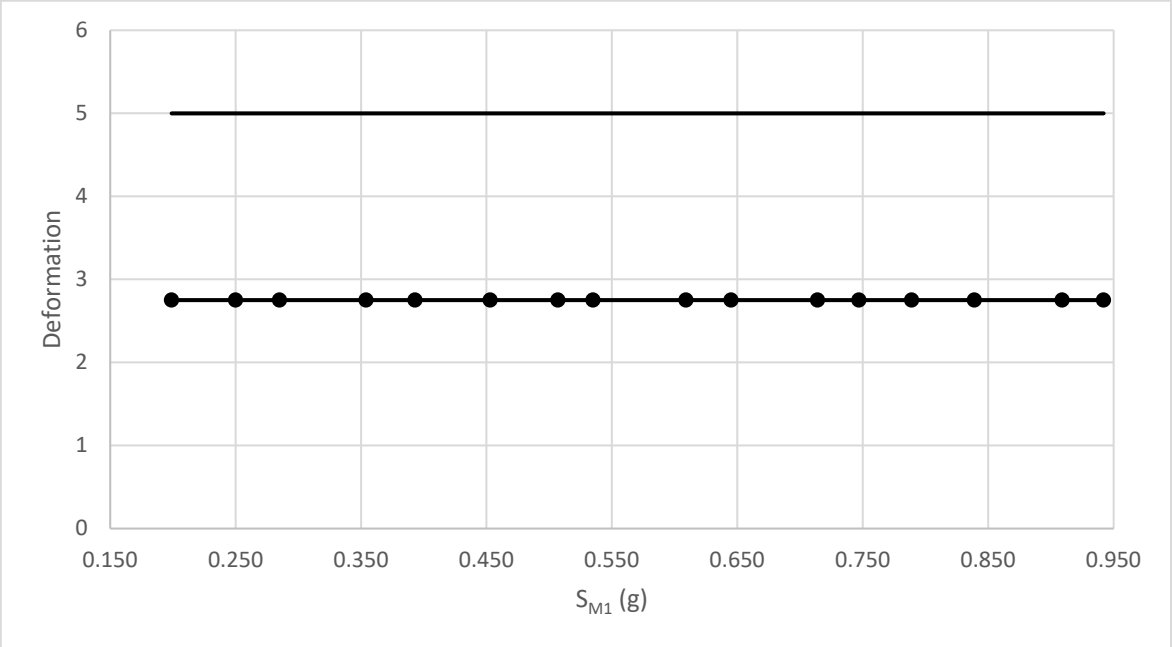


**Figure A5.** $S_{M1}$—Deformation ($P_{K1}$ b) (LRB) (Note: The major horizontal gridline corresponding to the value of 5 represents the strict regulatory upper limit for the deformation as mandated by TBEC 2018).

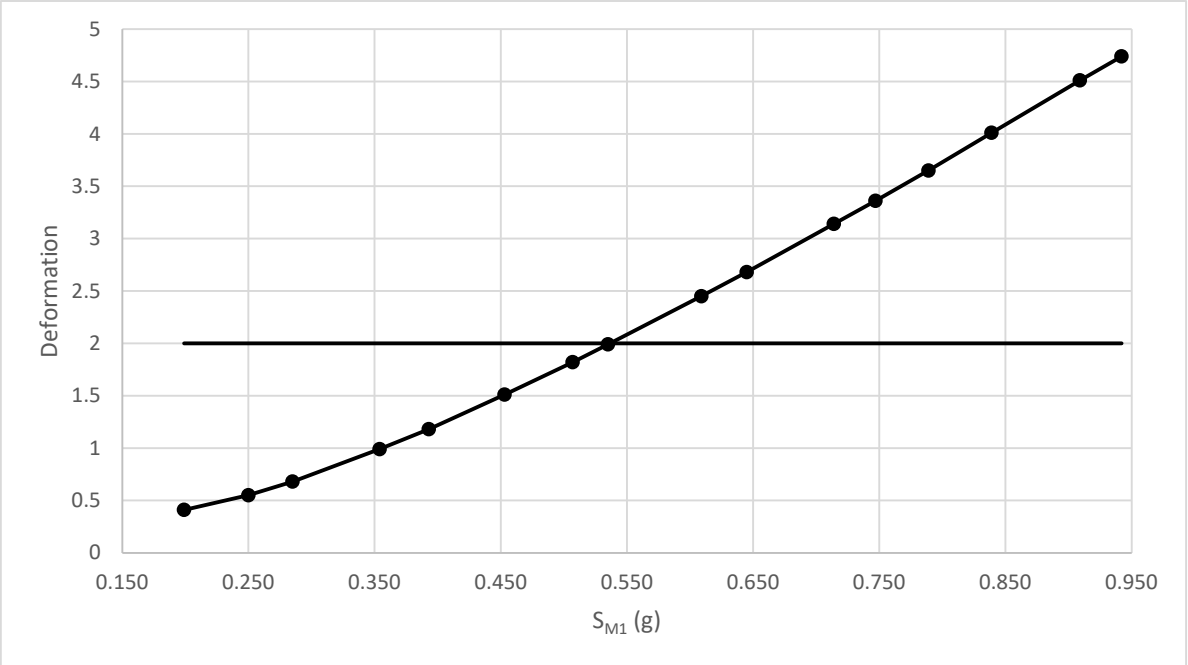


**Figure A6.** $S_{M1}$—Deformation ($P_{K2}$ a) (LRB) (Note: The major horizontal gridline corresponding to the value of 2 represents the strict regulatory upper limit for the deformation as mandated by TBEC 2018).

The increase in acceleration has no positive or negative impact on the deformation checks calculated under the $P_{K1}$ load combination. It is determined that the results remain within the safe region, staying below the upper limit thresholds of 3.5 to 5 (Figures A4 and A5).

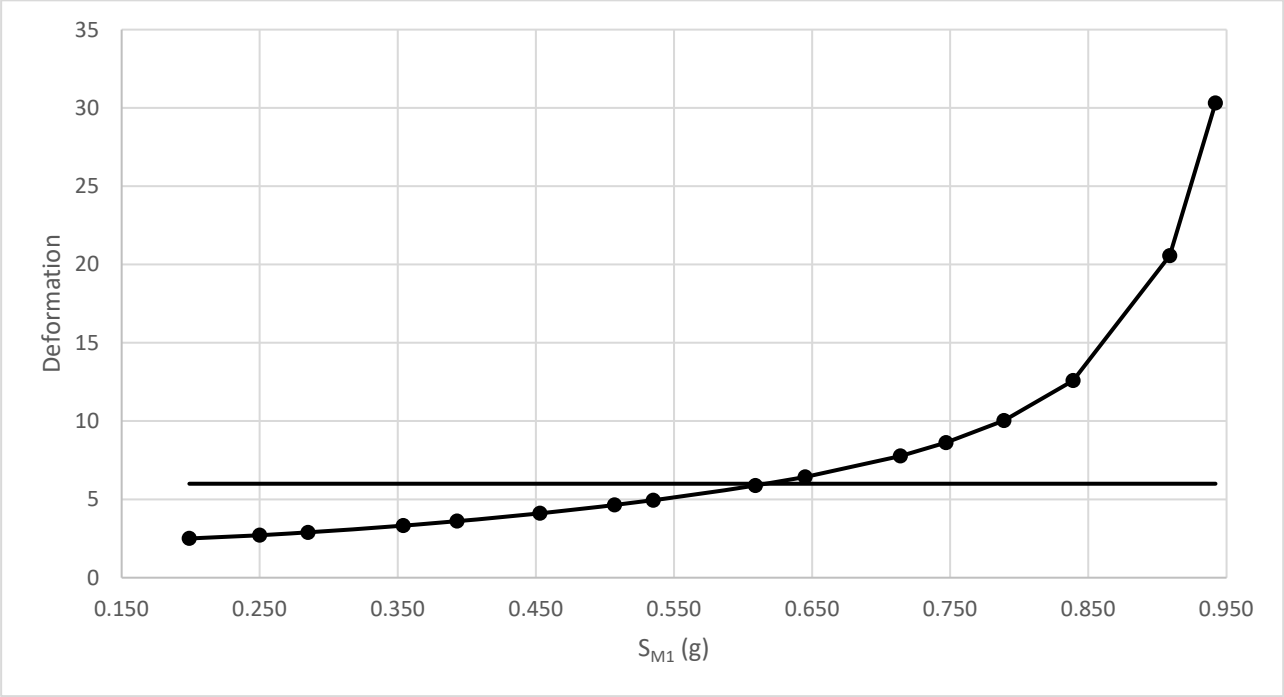


**Figure A7.** $S_{M1}$—Deformation ($P_{K2}$ b) (LRB) (Note: The major horizontal gridline corresponding to the value of 6 represents the strict regulatory upper limit for the deformation as mandated by TBEC 2018).

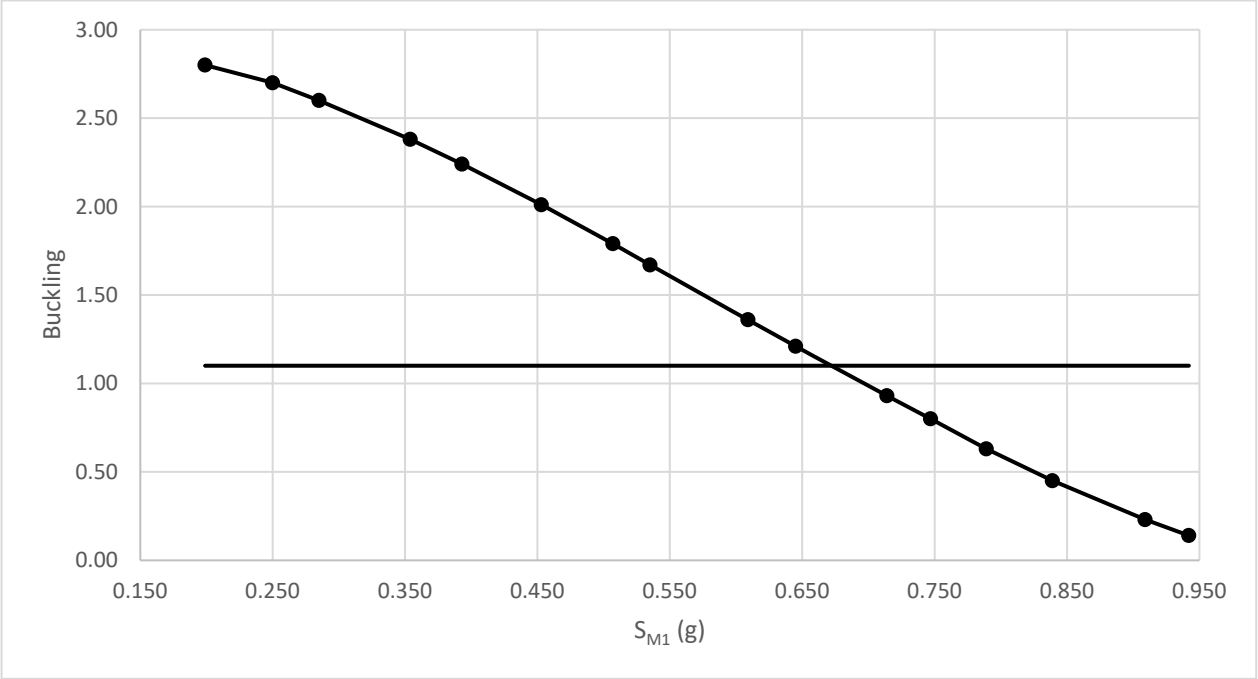


**Figure A8.** $S_{M1}$—Buckling (a) (LRB) (Note: The major horizontal gridline corresponding to the value of 1.1 represents the strict regulatory lower limit for the buckling as mandated by TBEC 2018).

The deformation checks performed under the $P_{K2}$ load combination become unsatisfied as acceleration values increase. The reason for this is the increase in the displacement that the isolator will undergo along with the acceleration increment (Figures A6 and A7).

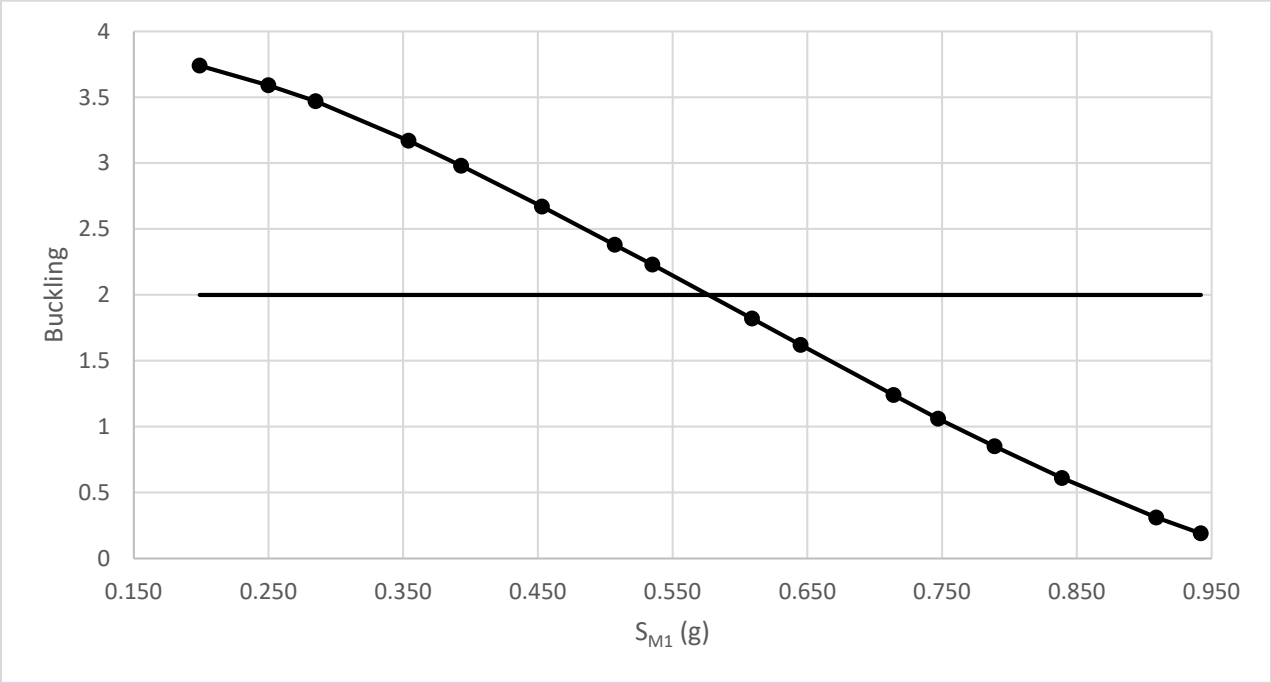


**Figure A9.** $S_{M1}$—Buckling (b) (LRB) (Note: The major horizontal gridline corresponding to the value of 2 represents the strict regulatory lower limit for the buckling as mandated by TBEC 2018).

The buckling checks for the LRB configuration fail to satisfy the safety criteria due to the progressive increase in isolator displacement demands that accompany rising acceleration levels (Figures A8 and A9).

To validate the accuracy of the proposed analytical model, a benchmark study was conducted using ETABS. A structural system was modeled with a 120 × 120 × 150 cm pedestal and a 50 cm high isolation unit (FPS/LRB). A vertical load of 3000 kN was applied to represent the seismic mass. The isolation unit was idealized by restricting rotational and vertical movements while allowing lateral displacements in the X and Y directions. Seismic loads were implemented using the 'User Coefficient' approach, where the base shear coefficient was calculated by scaling the spectral acceleration (incorporating the damping coefficient and a factor of 1.3). The comparison between the analytical results and ETABS simulations is presented in Table A1.

**Table A1.** Comparison of calculation tool and ETABS results for the benchmark model.

| Isolator Type | Parameter | Calculation Tool | ETABS | Difference |
|---|---|---|---|---|
| FPS | Period (s) | 4.00 | 4.00 | Negligible |
| FPS | Displacement (mm) | 425.32 | 425.30 | <0.01% |
| LRB | Period (s) | 2.43 | 2.43 | Negligible |
| LRB | Displacement (mm) | 303.2 | 302.90 | ~0.10% |

Note: The displacement values presented in Table A1 represent the uncoupled (lateral) displacement of the isolation system under the defined seismic load. In contrast, the displacement values reported throughout the main body of this manuscript refer to the torsional displacement ($D_{TM}$), which is obtained by applying a 1.1 multiplier to the uncoupled displacement to account for potential torsional effects.

## References


1. Kelly, J.M. Aseismic base isolation: Review and bibliography. *Soil Dyn. Earthq. Eng.* **1986**, *5*, 202–216. [CrossRef]
2. AFAD. *Turkish Building Earthquake Code (TBEC-2018)*; Ministry of Interior, Disaster and Emergency Management Presidency: Ankara, Turkey, 2018.
3. Wu, P.; Ou, J. Performance Analysis and Comparison of Two Base Isolation Systems with Super-Large Displacement Friction Pendulum Bearings. *Appl. Sci.* **2020**, *10*, 8235. [CrossRef]
4. Özer, E.; Inel, M.; Cayci, C. Seismic Behavior of LRB and FPS Type Isolators Considering Torsional Effects. *Res. Sq.* 2021, *Epub ahead of printing*. [CrossRef]
5. Hasan, Q.F.; Al-Mamany, D.A. Comparative Analysis of Lead Rubber Bearing and Friction Pendulum Bearing. *Solid State Technol.* **2020**, *63*, 2999–3010.
6. Nuraini, S.; Tambusay, A.; Suprobo, P. A comparative study of base isolation devices in light rail transit structure featured with lead rubber bearing and friction pendulum system. *MATEC Web Conf.* **2018**, *195*, 02013. [CrossRef]
7. Son, J.; Chin, W.; Cho, C.; Lee, J. Comparison of seismic resistance between LRB and FPB on energy dissipation per cycle and equivalent damping. *J. Disaster Sci. Manag.* **2025**, *1*, 9. [CrossRef]
8. Vibhute, A.S.; Bharti, S.D.; Shrimali, M.K.; Datta, T.K. Performance evaluation of FPS and LRB isolated frames under main and aftershocks of an earthquake. *Structures* **2022**, *44*, 1532–1545. [CrossRef]
9. Alasaf, E.; Öztürk, H. Sismik İzolatörlü Yapıların Tasarımına Etki Eden Faktörlerin İncelenmesi. *Duzce Univ. J. Sci. Technol.* **2022**, *10*, 2155–2164. [CrossRef]
10. Zulfakar, M.; Karakaş, A.İ. Farklı Sürtünmeli Sarkaç Tipi İzolatörlerin Yapı Sismik Davranışına Etkileri. *Duzce Univ. J. Sci. Technol.* **2022**, *10*, 1826–1837.
11. Öztürk, M. Hastanelerde Sürtünmeli Sarkaç Tipi İzolatörlerin Taşıyıcı Sisteme Etkisi. *Mühendislik Bilim. Ve Tasarım Derg.* **2025**, *13*, 570–581. [CrossRef]
12. Vilca, F.; Quiroz, L.; Torres-Matos, M. Performance assessment of lead rubber bearing system and triple friction pendulum system at Piura's hospital, in Peru. In Proceedings of the 16th World Conference on Earthquake, Santiago, Chile, 9–13 January 2017.
13. Mohan, A.; Jessie, A.; Glory, E.; Richard, T. Analysis of Reinforced Concrete and Steel Multi Storeyed Structures with Lead Rubber Bearing and Friction Pendulum Systems. *Nanotechnol. Percept.* **2024**, *20*, 193–201. [CrossRef]
14. Rajab, M.H.; Hasgur, Z.; Mahmoud, A.S. Dynamic Response of Multistory Reinforced Concrete Buildings Having Different Types of Isolators a Parametric Study. *Eurasian J. Sci. Eng.* **2024**, *10*, 8–15. [CrossRef]
15. Vibhute, A.S.; Bharti, S.D.; Shrimali, M.K.; Vern, S. Seismic Performance of Elastomeric and Sliding Friction Isolation System. *ASPS Conf. Proc.* **2022**, *1*, 815–819. [CrossRef]
16. Rajput, G.; Mishra, V. Performance of RC Building with Different base Isolators. *Int. J. Res. Appl. Sci. Eng. Technol.* **2022**, *10*, 1265–1269. [CrossRef]
17. Shiravand, M.R.; Ketabdari, H. Evaluating Seismic Response of Plan Irregular Buildings Using Combination of Lead Rubber Bearing Isolator and Friction Pendulum System. *J. Struct. Constr. Eng.* **2021**, *8*, 141–163.
18. Poornima, B.S.; Babu, B.S.J. Comparative Study on Seismic Response of Regular and Irregular RC Framed Buildings with HDRB, LRB and FPS Base Isolation Systems. *Int. J. Res. Appl. Sci. Eng. Technol.* **2019**, *7*, 805–813. [CrossRef]
19. Anand, G.; Suresh, G.S.; Pai, R. Seismic Evaluation of a Bridge with Different Isolators at Different Locations. *Int. J. Res. Appl. Sci. Eng. Technol.* **2019**, *7*, 591–602. [CrossRef]
20. Shen, Y.; El Naggar, M.H.; Zhang, D.; Huang, Z.K.; Du, X. Scalar- and vector-valued seismic fragility assessment of segmental shield tunnel lining in liquefiable soil deposits. *Tunn. Undergr. Space Technol.* **2025**, *155*, 106171. [CrossRef]
21. Shen, Y.; El Naggar, M.H.; Zhang, D.; Huang, Z.K.; Du, X. Optimal intensity measure for seismic performance assessment of shield tunnels in liquefiable and non-liquefiable soils. *Undergr. Space* **2025**, *21*, 149–163. [CrossRef]
22. Shen, Y.; El Naggar, M.H.; Zhang, D.; Huang, Z.K.; Du, X. Seismic resilience assessment of shield tunnel linings in sites susceptible to liquefaction. *Soil Dyn. Earthq. Eng.* **2026**, *207*, 110320. [CrossRef]
23. *ASCE/SEI 7-22*; Minimum Design Loads and Associated Criteria for Buildings and Other Structures. American Society of Civil Engineers: Reston, VA, USA, 2021.
24. Fago Sismik İzolasyon. Available online: https://fagosismikizolasyon.com/ (accessed on 4 June 2026).
25. TİS Teknolojik İzolasyon Sistemleri. Available online: https://tis.com.tr/ (accessed on 4 June 2026).
26. Mageba Group. Available online: https://www.mageba-group.com/tr/tr/ (accessed on 4 June 2026).
27. FIP MEC S.r.l. Available online: https://www.fipmec.it/en/ (accessed on 4 June 2026).
28. Hirun International Co., Ltd. Available online: https://hirun.eu/ (accessed on 4 June 2026).
29. Laibin Sismik İzolasyon Türkiye. Available online: https://www.laibin.com.tr/ (accessed on 4 June 2026).
30. MAURER SE. Available online: https://www.maurer.eu/en/ (accessed on 4 June 2026).
31. Bridgestone Corporation. Available online: https://www.bridgestone.com/products/diversified/antiseismic_rubber/ (accessed on 4 June 2026).

32. Dynamic Isolation Systems, Inc. Available online: https://www.dis-inc.com/ (accessed on 4 June 2026).
33. Özdekan Kauçuk İnşaat Yapı Proje Mühendislik A.Ş. Available online: https://www.ozdekan.com/ (accessed on 4 June 2026).
34. QuakeSafe Technologies Co., Ltd. (SAFETYINSIDE). Available online: https://www.safetyinside.cn/ (accessed on 4 June 2026).
35. Doshin Rubber Products (M) Sdn. Bhd. Available online: https://doshinrubber.com/ (accessed on 4 June 2026).
36. Pikasan Plastik Kauçuk Sanayi A.Ş. Available online: https://www.pikasan.com/ (accessed on 4 June 2026).
37. AFAD. *Türkiye Deprem Tehlike Haritası*; Afet ve Acil Durum Yönetimi Başkanlığı: Ankara, Turkey, 2018.
38. Computers and Structures, Inc. *ETABS: Integrated Building Design Software*; Computers and Structures, Inc.: Berkeley, CA, USA, 2024.
39. Sarfarazi, S.; Fulgione, M.; Fabbrocino, F. Physics-Informed Decision Framework for Reuse of Reclaimed Steel Members Under Uncertainty. *Metals* **2026**, *16*, 171. [CrossRef]
40. Constantinou, M.C.; Soong, T.T.; Dargush, G.F. *Property Modification Factors for Seismic Isolation Bearings*; MCEER Technical Report 99-0012; MCEER: New York, NY, USA, 1999.
41. Hamaguchi, H.; Aizawa, S.; Samejima, Y.; Kikuchi, T.; Suzuki, S.; Yoshizawa, T. A study of aging effect on a rubber bearing after about twenty years in use. *AIJ J. Technol. Des.* **2009**, *15*, 393–398. [CrossRef]
42. Kelly, J.M.; Konstantinidis, D.A. *Mechanics of Rubber Bearings for Seismic and Vibration Isolation*; John Wiley & Sons: Hoboken, NJ, USA, 2011.